

Non-Generic Dispersion of Excitons in the Bulk of WSe₂

R. Schuster,¹ Y. Wan,¹ M. Knupfer,¹ and B. Büchner^{1,2}

¹*IFW Dresden, Institute for Solid State Research, P.O. Box 270116, D-01171 Dresden, Germany*

²*Department of Physics, Technische Universität Dresden, 01062 Dresden, Germany*

(Dated: September 4, 2018)

We combine electron energy-loss spectroscopy (EELS) and density functional theory (DFT) calculations to study the dispersion and effective mass of excitons in the bulk of WSe₂. Our EELS data suggest substantial deviations from the generic quadratic momentum dependence along the ΓK -direction. From the DFT-derived Kohn-Sham states we deduce the EELS response without the inclusion of particle-hole attraction to study the possible role of the single-particle band structure on the exciton behavior. Based on this analysis we argue in favor of a strongly momentum dependent particle-hole interaction in WSe₂ and other group VI-transition-metal dichalcogenides.

I. INTRODUCTION

Transition-metal dichalcogenides (TMDCs) in general and the semiconducting group-VI representatives in particular have been investigated for decades¹. While originally of interest for their prototype role as anisotropic, quasi-2D semiconductors with indirect band gaps and their chemical and structural similarities to the metallic group V-relatives with charge-ordered and/or superconducting ground states, MoS₂ and related compounds like WSe₂ (re)gained substantial attention after it was realized that they exhibit a crossover from an indirect to a direct band gap as a function of layer number² yielding exceptionally large quantum yields in their photoluminescence spectra. This discovery can be considered a milestone for the field of optoelectronics in 2D semiconductors and it sparked a lot of research related to possible applications. In addition, it is by now well established that the fundamental physics of excitons – which are at the heart of the optical properties of TMDCs – is extraordinarily rich. This is related (i) to the honeycomb structure of the individual layers and (ii) the strong spin-orbit coupling (SOC) of the constituent atoms. By symmetry this dictates several remarkable observations, among them a finite contribution of the Berry curvature to the exciton dynamics^{3,4} and the so called valley degree of freedom^{5,6}.

While much is known about absorption and emission processes of TMDCs in the optical limit, i.e., the case of vertical transitions between occupied and unoccupied states^{7,8}, the response to probes allowing for non-vertical transitions between the valence- and conduction-states represents a widely open field. Here we employ a combination of electron-energy loss spectroscopy (EELS) in transmission together with first-principle calculations based on density-functional theory (DFT) to gain insight into the momentum dependence of exciton absorption in the bulk of WSe₂. This provides access to e.g. the effective mass of excitons and the q -dependence of particle-hole interactions.

II. EXPERIMENTS AND RESULTS

Electron energy-loss spectroscopy (EELS) in transmission⁹ is a bulk-sensitive scattering technique whose cross-section is proportional to the so called loss-function $L(\mathbf{q}, \omega) = \text{Im}(-1/\epsilon(\mathbf{q}, \omega))$, with $\epsilon(\mathbf{q}, \omega)$ the momentum- and energy-resolved dielectric function¹⁰. It has been successfully applied to investigate collective charge modes in numerous condensed-matter systems (see^{11,12} for an overview). Recently, the momentum dependence of excitons in other topical quasi-2D materials like MoS₂¹³ and black phosphorus¹⁴ has been successfully investigated with the same methodology. For the present experiments bulk-like thin ($d \approx 100$ nm) films of WSe₂ have been prepared by exfoliation from a single crystal purchased from “2D semiconductors” and measured in a purpose-built EELS spectrometer⁹ with energy and momentum resolutions of $\Delta E \approx 90$ meV and $\Delta q \approx 0.03 \text{ \AA}^{-1}$, respectively. All data were taken at a temperature of about 20 K to reduce thermal broadening.

In Fig. 1 we show the momentum dependent EELS intensity along the ΓK line of the hexagonal Brillouin zone (BZ).

It is well known that TMDCs exhibit a prominent splitting of the valence band (VB)-edge around the K -point, the origin of which is to some extent a matter of controversy but is believed to originate from SOC for the monolayer (ML) and from a combination of SOC and inter-layer hybridization for few-layer and bulk systems¹⁵. The size of this splitting varies for different representatives and has been calculated to about 0.5 eV for WSe₂¹⁶. This value is confirmed experimentally by angle-resolved photoemission¹⁷ and our own calculations (see below). The spectral shape of the optical response in TMDCs is a consequence of the superimposed joint-densities of states for the two VBs at the K -point with the conduction band (CB) minimum¹⁵. On top of these two step-function-like continua, prominent excitonic features emerge due to sizable particle-hole attraction which are known to be strongly enhanced upon approaching the ML limit. Compared to MoS₂¹³ the higher value of the SOC at the K -point and a suppressed single-particle continuum, enhances the visibility of the exciton features of WSe₂

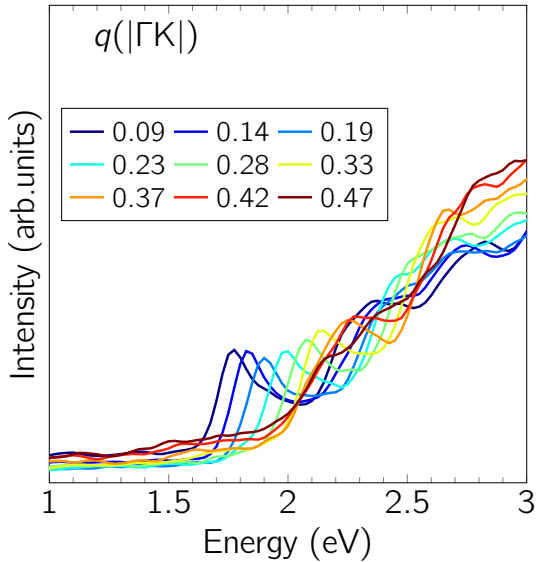


Figure 1: (Color online) Momentum dependent EELS intensity of bulk WSe₂ along ΓK .

and allows to trace the momentum dependent exciton absorption up to much higher q -values. Consequently, the data shown in Fig. 1 suggest a substantial exciton dispersion to be discussed below.

To retrieve the complex dielectric function $\epsilon(\omega) = \epsilon_1(\omega) + i\epsilon_2(\omega)$, EELS data have been corrected for contributions from the elastic line and multiple scattering and normalized to yield $\epsilon_1(\omega = 0)$ in agreement with earlier reports¹⁸. The resulting curves for the real and imaginary part of the dielectric function are shown in Fig. 2.

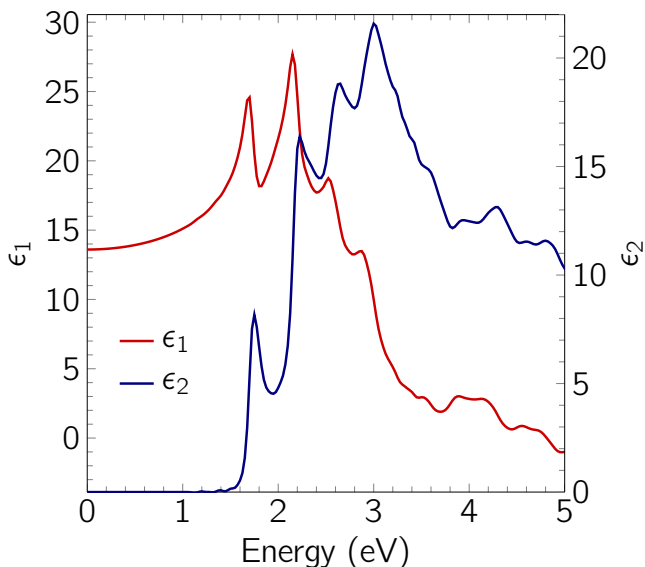


Figure 2: (Color online) Dielectric function for WSe₂ as obtained from a KKA of the measured EELS intensity.

The first absorption peak lies at 1.75 eV which is in excellent agreement with previous reports^{19,20}.

Note that the first peak in the absorption spectrum (proportional to $\epsilon_2(\omega)$) occurs at 1.75 eV. Given that the calculated single-particle gap at the GW-level amounts to about 1.75 eV²¹ the exciton binding energy of bulk-WSe₂ is very small²⁰ which makes an interpretation of the observed particle-hole pair in terms of a Wannier-Mott like state appealing. This behavior is to be contrasted with the prediction of a much higher exciton binding energy of 0.9 eV in the ML of WSe₂²². This is supported by calculations for the spread of the excitonic wavefunction in the bulk of the related MoS₂-system¹⁵. Note, however that the coincidence between excitonic binding energy and the corresponding level of (de)localization is ambiguous for the case of MLs as in the 2D limit screening is strongly reduced which always yields a sizable exciton binding energy, independent of the spatial extension of the particle-hole pair²³.

In the case of a weakly-bound Wannier-Mott exciton, the dispersion of the two-particle wavepacket is given within the so called effective mass approximation (EMA)²⁴ by

$$E(q) = \frac{\hbar^2 q^2}{2M^*} + E_0 \quad (1)$$

with the effective exciton mass given as the sum of the effective electron- and hole-mass-values $M^* = m_e^* + m_h^*$. Although it has been shown recently that the EMA must be augmented to capture the contribution from a finite Berry-curvature^{3,4} for excitonic states with non-zero angular momentum, we emphasize that our energy resolution is not sufficient to observe excited states in the Rydberg series and we take Eq. (1) to describe our experimental data shown in Fig. 1. Fig. 3 contains the experimentally observed exciton dispersion as obtained from the low-energy edges of the data shown in Fig. 1 together with a low q -fit according to the EMA. As can be seen, in the vicinity of the BZ center the EMA yields excellent agreement with the experimental data with a derived exciton mass of $M^* \approx 0.91 m_0$ with the free electron mass m_0 . In contrast to this, for higher q -values there is an increasing discrepancy between the model and the data. In particular, we find a downturn of the dispersion at $q \sim 0.4 |\Gamma K|$ which is in stark contrast to the monotonic behavior predicted within the EMA.

Deviations from the generic quadratic momentum dependence of the exciton dispersion are well expected in the case of degenerate bands. It was realized early on that the canonical coordinate transformation to solve the Schrödinger equation for the two-particle state is not possible in the case of degenerate bands²⁵. This circumstance is known to yield deviations from the simple parabolic exciton band structure²⁶. While the valence band edges at the K -point of the hexagonal BZ are strongly split because of the strong SOC, the CB minima are nearly (cf. our band structure calculations discussed below) degenerate at the same point in the BZ. But even if this degeneracy was present, it is lifted already for small deviations from

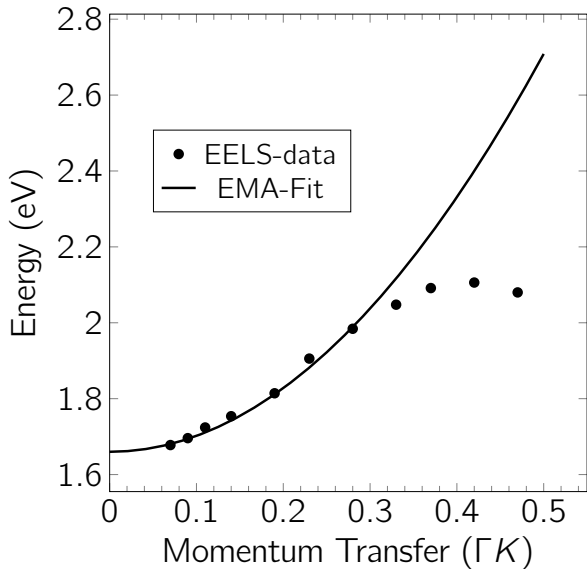


Figure 3: The dispersion of the lowest energy structure in the data shown in Fig. 1 together with corresponding low- q fits of the generic form $E(q) = E_0 + A \cdot q^2$. From the fit we obtain an effective exciton mass of $M \approx 0.91 m_0$. Note the marked discrepancy for higher momentum values and in particular the downturn of the data points for $q \sim 0.4 |\Gamma K|$.

the high-symmetry point, and we therefore exclude this effect as being responsible for the non-parabolic shape observed in Fig. 3.

Another possible source of a non-generic exciton momentum dependence might be an interference with the absorption caused by interband transitions. To investigate this issue we have performed first-principle calculations with the FPLO package²⁷ including SOC and employing the generalized gradient approximation (GGA) as parametrized by Perdew, Burke and Ernzerhof²⁸. As input we used the crystal structure given in²⁹ except for the in-plane lattice constant which we derived *in-situ* from our own electron diffraction data. The total density was converged on a grid of $24 \times 24 \times 12$ irreducible k -points. The calculated single-particle band structure is shown in Fig. 4.

In agreement with previous reports^{16,21}, our DFT calculations yield an indirect gap of 0.93 eV, the VB maximum at the Γ -point (lying ~ 70 meV above the maximum at the K -point), a substantial (~ 520 meV) SO-induced splitting of the VB around the K -point and the CB-minimum approximately halfway along the ΓK -line. The values for the effective masses derived from our calculations are given in Tab. I.

As can be seen, our DFT calculations *overestimate* the exciton effective mass derived from our EELS data shown in Fig. 3. The origin of this discrepancy is unknown at the moment. Usually, DFT tends to underestimate effective mass values which can be improved by quasiparticle

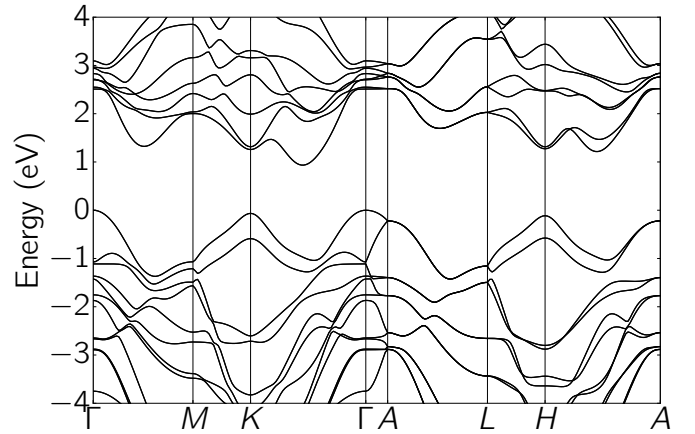


Figure 4: GGA-derived single-particle band structure for WSe_2 . The zero of the energy axis was set to the VB maximum at the Γ -point.

Table I: Effective mass values derived from a quadratic expansion of the Kohn-Sham states shown in Fig. 4 around the K -point. All values are in units of the free electron mass m_0 .

Quasiparticle	Effective Mass
electron (m_e^*)	0.548
light hole (m_{LH}^*)	0.465
heavy hole (m_{HH}^*)	0.607
exciton ($M^* = m_e^* + m_{LH}^*$)	1.01

corrections in terms of more elaborate GW-calculations. However, from corresponding data for the TMDCs it is known that the curvature of the Kohn-Sham derived band structure (in particular those from the VB region) are stable against the self-energy corrections induced by the GW-term^{15,21}. Therefore effective masses obtained within DFT are supposedly close to the ones obtained from GW-renormalized bands.

To investigate the possible effect of interband transitions on the exciton dispersion we define a simplified one-dimensional (along the ΓK -cut) model for the susceptibility

$$\chi_0(q, \omega) = 2 \sum_{v,c,k} \frac{1}{\omega - (\epsilon_{k+q}^c - \epsilon_k^v) + i\delta} \quad (2)$$

from which we can derive an effective dielectric function according to

$$\frac{1}{\bar{\epsilon}(q, \omega)} = 1 + \frac{1}{q^2} \chi_0(q, \omega). \quad (3)$$

Here, the $\epsilon_k^{c(v)}$ correspond to conduction (valence) Kohn-Sham bands derived from our GGA-calculations shown in Fig. 4, $q, k \in (0, |\Gamma K|)$ and the sum runs over all VB and CB states (except for spin-degeneracy which causes the

factor of two) up to a defined energy cut-off (3.5 eV in the present case). The reason for the latter is to keep transitions originating from particular q -points discernible. If the cut-off is chosen too high, all features become smeared in a broad continuum preventing a straightforward mode assignment. This model contains two essential assumptions: (i) The excitonic bands follow the Kohn-Sham single-particle bands $\epsilon_k^{c(v)}$, i.e. we neglect particle-hole attraction. While this appears unphysical at first sight, we justify this by the very small exciton binding energy as discussed above. (ii) The matrix element mediating the transitions between the VB and the CB, which in a more realistic model would enter the numerator of Eq. (2), is constant for $q \parallel \Gamma K$. This is motivated by the observation that the orbital weight of the VB and CB states in TMDCs vary only moderately along the ΓK -direction³⁰. The result of our model calculation is shown in Fig. 5.

From the inset of Fig. 5 for $q \rightarrow 0$ one can identify several prominent structures in the two-particle spectrum. Therein the lowest (highest) lying structures at energies $E_I \approx 1.34$ eV, ($E_{II} \approx 2.53$ eV) correspond to vertical transitions in the $K(\Gamma)$ -point region of the BZ. In the following we are only concerned with the former. Compared to the experimental data shown in Fig. 2 its calculated energy position lies at much lower energies. This is a consequence of the well known underestimation of the band gap in DFT like calculations. As can be seen from Fig. 5, upon increasing the momentum transfer, this feature first disperses quadratically to higher energies until $q \sim 0.18 \Gamma K$ where it starts to hybridize with a downward dispersing mode which leads to an effective red-shift of the lowest feature. The origin of this downturn lies in the local maximum of the lowest CB along the ΓK -line (cf. Fig. 4). While it is tempting to identify this redshift with the corresponding experimental observation shown in Fig. 3 we emphasize that there is a large mismatch in the momentum location of these maxima.

We therefore also exclude interband transitions as the cause for the peculiar momentum dependence shown in Fig. 3. Consequently our data are suggestive of a strong momentum dependence of the particle-hole attraction which is supposed to renormalize the denominator of the two-particle response function in Eq. (2). Indeed, recently the momentum dependence of the exchange interaction has been shown to play a prominent role in the interpretation of the exciton character in MLs of TMDCs²³. In particular, it has been argued that the momentum dependence of the exchange interaction leads to a flattening of the exciton band structure away from the zone center if the exciton wave function is localized in the limit $q \rightarrow 0$. From our observation of a strongly non-generic exciton dispersion in the bulk of WSe₂ we are led to speculate that already in the bulk-limit the interaction of the particle-hole pair is non-trivial. WSe₂ provides an ideal platform to study this behavior as the enhanced SOC and the overall shape of the interband continuum allows to track the exciton up to much higher momentum values compared to the related MoS₂.

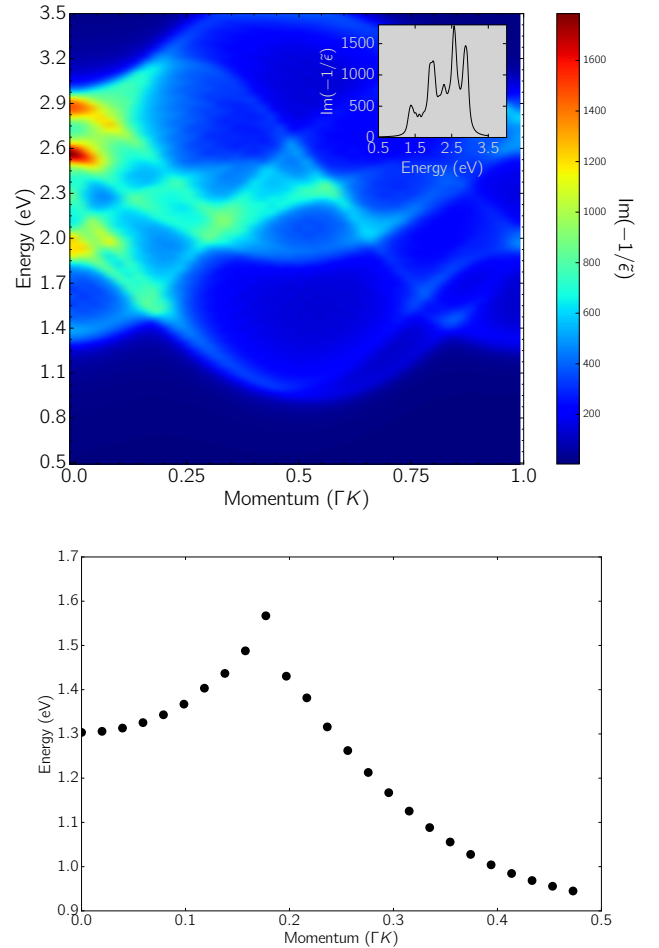


Figure 5: (Color online) Top Panel: $\text{Im}(-1/\tilde{\epsilon}(q, \omega))$ as calculated from the simplified model along the ΓK line according to Eq. (3). A phenomenological broadening of $\delta = 50$ meV has been employed. The inset shows $\text{Im}(-1/\tilde{\epsilon}(0, \omega))$. Bottom panel: The dispersion obtained from the edge of the lowest-energy feature. Note the prominent maximum at $q \sim 0.18 |\Gamma K|$

III. SUMMARY

In summary, we investigated the dispersion of excitons in the bulk of WSe₂ with EELS. In the vicinity of the BZ center we observe a quadratic momentum dependence which is the generic behavior expected for a Wannier-Mott like state. Upon increasing the momentum transfer there are, however, substantial deviations from this picture. From a comparison with the optical response generated by uncorrelated interband transitions calculated from density-functional theory we argue in favor of a non-trivial particle-hole interaction in the bulk of TMDCs.

IV. ACKNOWLEDGMENTS

We highly appreciate technical support from R. Hübel, S. Leger and M. Naumann and helpful guidance from T. Ritschel concerning the DFT calculations.

-
- ¹ J. A. Wilson and A. D. Yoffe, *Adv. Phys.* **18**, 193 (1969).
² K. F. Mak, C. Lee, J. Hone, J. Shan, and T. F. Heinz, *Phys. Rev. Lett.* **105**, 136805 (2010).
³ J. Zhou, W.-Y. Shan, W. Yao, and D. Xiao, *Phys. Rev. Lett.* **115**, 166803 (2015).
⁴ A. Srivastava and A. Imamoglu, *Phys. Rev. Lett.* **115**, 166802 (2015).
⁵ H. Yu, X. Cui, X. Xu, and W. Yao, *Natl. Sci. Rev.* **2**, 57 (2015), <http://nsr.oxfordjournals.org/content/2/1/57.full.pdf+html>.
⁶ X. Xu, W. Yao, D. Xiao, and T. F. Heinz, *Nat Phys* **10**, 343 (2014).
⁷ H. Zeng and X. Cui, *Chem. Soc. Rev.* **44**, 2629 (2015).
⁸ K. Matsuda, *J. Phys. Soc. Jpn.* **84**, 121009 (2015), <http://journals.jps.jp/doi/pdf/10.7566/JPSJ.84.121009>.
⁹ J. Fink, *Adv. Electron. Electron Phys.* **75**, 121 (1989).
¹⁰ K. Sturm, *Z. Naturforsch.* **48a**, 233 (1993).
¹¹ F. Roth, A. König, J. Fink, B. Büchner, and M. Knupfer, *J. Electron Spectrosc. Relat. Phenom.* **195**, 85 (2014).
¹² J. Fink, M. Knupfer, S. Atzkern, and M. S. Golden, *J. Electron Spectrosc. Relat. Phenom.* **117-118**, 287 (2001).
¹³ C. Habenicht, M. Knupfer, and B. Büchner, *Phys. Rev. B* **91**, 245203 (2015), [1505.06401](https://doi.org/10.1103/PhysRevB.91.245203).
¹⁴ R. Schuster, J. Trinckauf, C. Habenicht, M. Knupfer, and B. Büchner, *Phys. Rev. Lett.* **115**, 026404 (2015).
¹⁵ A. Molina-Sánchez, D. Sangalli, K. Hummer, A. Marini, and L. Wirtz, *Phys. Rev. B* **88**, 045412 (2013).
¹⁶ R. Roldán, J. A. Silva-Guillén, M. P. López-Sancho, F. Guinea, E. Cappelluti, and P. Ordejón, *Ann. Phys.* **526**, 347 (2014).
¹⁷ J. M. Riley, F. Mazzola, M. Dendzik, M. Michiardi, T. Takayama, L. Bawden, C. Granerod, M. Leandersson, T. Balasubramanian, M. Hoesch, T. K. Kim, H. Takagi, W. Meevasana, P. Hofmann, M. S. Bahramy, J. W. Wells, and P. D. C. King, *Nat Phys* **10**, 835 (2014).
¹⁸ A. R. Beal, W. Y. Liang, and H. P. Hughes, *J. Phys. C* **9**, 2449 (1976).
¹⁹ A. R. Beal and W. Y. Liang, *J. Phys. C* **9**, 2459 (1976).
²⁰ A. Anedda, E. Fortin, and F. Raga, *Can. J. Phys.* **57**, 368 (1979), <http://dx.doi.org/10.1139/p79-048>.
²¹ H. Jiang, *J. Phys. Chem. C* **116**, 7664 (2012).
²² A. Ramasubramaniam, *Phys. Rev. B* **86**, 115409 (2012).
²³ P. Cudazzo, L. Sponza, C. Giorgetti, L. Reining, F. Sottile, and M. Gatti, *Phys. Rev. Lett.* **116**, 066803 (2016), [1512.09332](https://doi.org/10.1103/PhysRevLett.116.066803).
²⁴ P. Y. Yu and M. Cardona, *Fundamentals of Semiconductors* (Springer).
²⁵ G. Dresselhaus, *J. Phys. Chem. Solids* **1**, 14 (1956).
²⁶ M. Altarelli and N. O. Lipari, *Phys. Rev. B* **15**, 4898 (1977).
²⁷ K. Koepf and H. Eschrig, *Phys. Rev. B* **59**, 1743 (1999).
²⁸ J. P. Perdew, K. Burke, and M. Ernzerhof, *Phys. Rev. Lett.* **77**, 3865 (1996).
²⁹ W. Schutte, J. D. Boer, and F. Jellinek, *J. Solid State Chem.* **70**, 207 (1987).
³⁰ E. Cappelluti, R. Roldán, J. A. Silva-Guillén, P. Ordejón, and F. Guinea, *Phys. Rev. B* **88**, 075409 (2013).